Available online at www.sciencedirect.com

ScienceDirect

Nuclear Physics A 933 (2015) 306–324

NUCLEAR PHYSICS A

www.elsevier.com/locate/nuclphysa

Finite size effects in neutron star and nuclear matter simulations

P.A. Giménez Molinelli *, C.O. Dorso

Departamento de Física, Facultad de Ciencias Exactas y Naturales, Universidad de Buenos Aires and IFIBA, CONICET, Cuidad Universitaria, Buenos Aires 1428, Argentina

Received 4 April 2014; received in revised form 31 October 2014; accepted 5 November 2014

Available online 13 November 2014

Abstract

In this work we study molecular dynamics simulations of symmetric nuclear and neutron star matter using a semi-classical nucleon interaction model. Our aim is to gain insight on the nature of the so-called "finite size effects", unavoidable in this kind of simulations, and to understand what they actually affect. To do so, we explore different geometries for the periodic boundary conditions imposed on the simulation cell: cube, hexagonal prism and truncated octahedron. For nuclear matter simulations we show that, at sub-saturation densities and low temperatures, the solutions are non-homogeneous structures reminiscent of the "nuclear pasta" phases expected in neutron star matter simulations, but only one structure per cell and shaped by specific artificial aspects of the simulations—for the same physical conditions (i.e. number density and temperature) different cells yield different solutions. The particular shape of the solution at low enough temperature and a given density can be predicted analytically by surface minimization. We also show that even if this behavior is due to the imposition of periodic boundary conditions on finite systems, this does not mean that it vanishes for very large systems, and it is actually independent of the system size. We conclude that, for nuclear matter simulations, the cells' size sets the only characteristic length scale for the inhomogeneities, and the geometry of the periodic cell determines the shape of those inhomogeneities.

To model neutron star matter we add a screened Coulomb interaction between protons, and perform simulations in the three cell geometries. Our simulations indeed produce the well known nuclear pasta, with (in most cases) several structures per cell. However, we find that for systems not too large results are affected by finite size in different ways depending on the geometry of the cell. In particular, at the same certain physical conditions and system size, the hexagonal prism yields a single structure per cell while the cubic and truncated octahedron show consistent results, with more than one structure per cell. For systems of the size studied in this work these effects are still noticeable, but we find evidence to support

* Corresponding author.
E-mail address: pagm@df.uba.ar (P.A. Giménez Molinelli).

http://dx.doi.org/10.1016/j.nuclphysa.2014.11.005

that the dependence of the results on the cell geometry becomes smaller as the system size is increased. When the Coulomb interaction is present, the competition between opposing interactions of different range results in a proper, physically meaningful length scale that is independent of the system size and periodic cell of choice. Only under these conditions "finite size effects" will vanish for large enough systems (i.e. cells much larger than this characteristic length). Larger simulations are in order, but our computational capabilities forbid it for the time being.

Keywords: Nuclear astrophysics; Nuclear matter phase transition; Molecular dynamics simulations; Finite size effects

1. Introduction

In the inner crust of neutron stars, nucleons (protons and neutrons) exist at low temperatures and densities. They are also embedded in a (charge neutralizing) degenerate electron gas. Under those conditions, instead of forming the usual quasi-spherical nuclei found in Earth ("normal" nuclei), nucleons behave like a complex fluid called Neutron Star Matter (NSM). In NSM, nucleons attract each other through the short-ranged nuclear interaction while protons, in addition, repel each other through the Coulomb interaction screened by the electron gas. Studies of low density NSM have found that the attractive-repulsive interplay of nuclear and Coulomb forces may drive nucleons to take non-uniform configurations which are collectively known as "nuclear pasta" [1].

1.1. Non-homogeneous phases of neutron star matter

In the context of nuclear systems, the existence of nuclear pasta was early proposed in a pioneering work by Ravenhall et al. [1]. There the authors argued that the interplay between surface and Coulomb self-energies, which at low densities produce the almost spherical normal nuclei, is modified when those nuclei form a dense lattice:

> (...) ordinary nuclei are more or less spherical. While not disputing this fact, we observe that in the density range we have cited, where the fraction of space filled by dense matter, u, ranges from 0.1 to 1, the contribution to the Coulomb energy of the system coming from neighboring nuclei (the so-called Coulomb lattice energy) rivals in importance the nuclear Coulomb self-energy.

To analyze the effect of the long range Coulomb interaction at sub-saturation densities they used a static compressible liquid drop model in the Wigner–Seitz approximation. The Wigner–Seitz approximation was devised to simplify calculations in a charge neutral lattice of arbitrary shape. It consists in replacing the charge neutral unit cell with another cell of a simple geometry, adequate for the chosen lattice dimensionality: a sphere in $3D$, a cylinder in $2D$ or a slab in $1D$. Lattice Coulomb energy is included implicitly by making the electrostatic potential vanish at the cell's boundary.

The calculations from [1] were made at zero temperature with a proton fraction $x = 0.3$. Authors assumed nucleons to be arranged in dense matter regions at saturation density ρ_0 but filling only a fraction of space. With this model they found that for a rather wide range of densities, NSM arranged in these idealized lattice geometries is more stable than uniform matter or

normal nuclei. As described by the authors, these non uniform phases range in order of increasing density from spherical ($3D$) "nuclei", cylindrical ($2D$) "nuclei", passing through a slab-like "nuclei", then to cylindrical "bubbles", spherical "bubbles", until finally at $\rho \approx 0.85\rho_0$ the system becomes uniform.

For each geometry the unit cell has a characteristic length r_c which is the radius of the sphere for $3D$ and the cylinder in $2D$. For the $1D$ lattice, it is the half width of the lattice parameter. Although the value of this parameter is not explicitly given, it is $\sim$10 fm—the width of the slabs that are the stable solution at volume fraction 0.5.

While groundbreaking, this work assumed possible shapes *a priori*. Moreover, the authors make no mention to a possible dependence of the results on the unit cell's size r_c. And since surface effects are supposed to be at the core of the whole phenomenon, such drawback might be critical.

Later on, to address this criticisms, Williams and Koonin improved the calculations [2] by allowing NSM to assume any arbitrary configuration within a cubic unit cell of side L (not to be mistaken with a Wigner–Seitz cell) under periodic boundary conditions (PBC). To allow for arbitrary configurations they divided the unit cell into a cubic lattice. The local number density of symmetric NSM at each site was relaxed to minimize an energy functional. The energy functional was divided explicitly and *a priori* in bulk, surface and Coulomb terms. For the proton–proton Coulomb interaction, the zero temperature Thomas–Fermi approximation was employed [3], under which the Coulomb potential is screened and takes the form:

$$V_{TF}(r) = \mathrm{q}^2 \frac{e^{-r/\lambda}}{r}$$

Since the Thomas–Fermi screening length is much larger than any other length scale involved, the authors argued that it is a good approximation to include electrons as a uniform background of negative charge, just to neutralize the system. The minimization of energy was carried out through a careful and complex procedure which involved variation of the local number density, the overall mean density and the unit cell's size. Due to computational limitations, the largest cell size considered was of $L = 32$ fm and the lattice spacing fixed at 1 fm. Also, the authors state that the choice of a cubic cell was made solely for computational convenience but other geometries would be valid. They are aware that this poses a bias on the possible density configurations they may obtain, but they also state that their calculations contemplate all possible density configurations which have periodic cubic symmetry.

With this model their results include, in addition to the original "pasta", a new shape (dubbed "cross") which they describe as a slab with regular holes. According to the authors, this new shape is an energy minimum only for a very small range of densities, and so shallow that it "would be washed out by finite temperature" (sic). Most interestingly, by increasing the mean density adiabatically this phase transforms into a regular slab, but in a larger cell. Although the authors do not mention it, this is explicit proof that, at least within this model, the shape that minimizes the energy depends on the arbitrary cell size. Furthermore, in order to find the true minimum energy configuration at a given density, several system sizes must be explored to avoid (or at least exhibit) finite size effects.

More recently, Monte Carlo and Molecular Dynamics simulations have become popular tools to study the behavior of NSM at sub-saturation densities [4–6,9,15,16]. These simulations usually consider (n, p, e) matter (neutrons, protons and electrons only) at a fixed number of particles, volume and temperature. Electrons, however, are never included explicitly in the simulations but are treated either as an ideal Fermi gas or a uniform background charge distribution for the

double purpose of achieving charge neutrality and screening the Coulomb interaction between protons.

The advantage of using a dynamical and, for want of a better word "microscopic" approach, is that nucleons are treated individually instead of dealing with local densities. And instead of artificially splitting the energy contributions *a priori* in bulk, surface and Coulomb terms, pairwise interaction potentials are used. The dynamics itself then arranges the nucleons in whatever shape is optimal for the model without any bias, except for the geometry and size of the simulation cell.

1.2. Other systems with non-uniform phases

Similar non-homogeneous structures are found in soft condensed matter [19] and are, actually, inherent to any system with competing interactions of different ranges (see [21,22] and references therein). Phenomenologically this usually manifests as a competition between bulk and surface (or interfacial) energies, which is settled by adopting a geometry such that its surface is minimal [23], subject to certain constraints.

The formation of nuclear pasta has also been described as a frustration of surface minimization produced by Coulomb interaction [21]. In any case, even partial or frustrated, surface minimization seems to lie at the core of the nuclear pasta phenomenon.

In mathematics the problem of finding the minimal surface subject to certain boundary conditions, is known as the "Plateau" problem [24]. A minimal surface can be defined as a surface with zero average curvature at every point. All the usual pasta, plus Williams and Koonin's Crosses, CMD's "jungle-gym" [9] (known as the plumber's nightmare in polymer physics), as well as the Gyroid and Double Diamond structures proposed in [18] are solutions with cubic symmetry to this well studied problem [28]. For example, HF models for NSM [17,27] yield the so-called Schwarz's P-Surface and D-Surface [28]. CMD's jungle-gym also resembles the Schwarz's P-Surface. Watanabe et al. report that with QMD they find several unspecified "triply periodic" structures [20].

As far as we know, every simulation of NSM was performed in cubic cells under PBC. And every pasta-like structure found in those simulations is actually a triply periodic minimal surface of cubic symmetry. As such, they may be constrained to some extent by the geometry and symmetries of the primitive cell, not only by its size. Most notably, whenever a model yields only one structure per cell [27]. In light of this, exploring cell geometries with different symmetries might be enlightening.

1.3. Simulations and finite size considerations

In particle-based simulations finite size is always a concern, but it is assumed that for large enough cells, the so-called "finite size effects" would become negligible. That, however, is not always true. At least not for every observable. In [10,12,13], for example, grand canonical Monte Carlo simulations are performed for a Lennard–Jones fluid at densities that correspond to phase coexistence in the (mean field) Van der Waals approximation. The liquid phase in these simulations appears ordered in non-homogeneous structures eerily reminiscent to those observed in systems with competitive interactions, but arising exclusively from finite size effects related to Periodic Boundary Conditions (PBC) [11]. We shall refer to those structures as "pseudo-pasta" to distinguish them from "true" pasta, that which arises in systems with competing interactions.

In [13], the authors show both analytically and numerically that at the liquid–vapor coexistence region of a Lennard–Jones fluid, the liquid phase is shaped in a very distinct way for a

given density and temperature. They assume a cubic cell under PBC and show that if that cell is large enough, the shapes of these pseudo-pasta are limited to one spherical drop, one cylindrical rod, one slab, one cylindrical hole or one spherical hole in the simulation cell (in order of increasing number density). Small transitional density regions exist due to interfacial effects related to the finite range of the interactions, but these effects become smaller as system size is increased and/or temperature is lowered. In the limit of infinitely large and/or cold systems ($L \to \infty$) the transition densities can be calculated exclusively from surface minimization.

This behavior is observed for systems of various sizes and, based on scaling properties of the Landau free energy, it is shown that in the $L \to \infty$ limit the size dependence of every *intensive* quantity vanishes. This is so because their size dependence appears explicitly through surface to volume ratios which naturally (but slowly) become negligible as the size is increased. But most notably, it is also shown in the limit $L \to \infty$ limit, the transition from uniform liquid to uniform vapor is made in discontinuous steps, passing through the same sequence of shapes expected in NSM (spherical bubble, cylindrical bubble, slab, rod and spherical droplet) but only one per simulation cell.

Unaware of most of these works, in [11] we found the same structures in simulations of both Lennard–Jones and symmetric NM for several semi-classical interaction models for the nuclear interaction. Our simulations were done at constant volume and almost zero temperature. We explained these pseudo-pasta structures as minimal surface configurations under cubic PBC, and shown them to be the most stable configuration independently of system size (consistently with the results from [13]). Thus, we concluded that these behavior is intrinsic to the *finite* size of simulations under PBC, and not due to the system being *small*, as is usually interpreted. This scenario is very often ignored but is inherent to simulations of any LJ-like system.

With this background, it is feasible that at least some of the pasta structures found in NSM simulations (with Coulomb interaction) might be biased by finite size. More so since only cubic PBC were ever used, and every pasta ever reported has cubic symmetry and periodicity. It is even possible that some may be entirely an artifact of the simulation itself, specially if the size of the simulation cell is small, or for models that produce only one structure per cell, such as [17].

And in any case, ignoring these effects may lead to wrong estimates of the true scale of the density fluctuations, which in the case of nuclear pasta is of paramount importance [6].

1.4. Aim and organization of this work

In this work we aim to show that in molecular dynamics simulations of symmetric nuclear matter, at sub-saturation densities and low temperatures, performed under periodic boundary conditions, the spatial configuration is determined exclusively by the enforced periodicity of the cell. Even though these are finite size effects, they do not vanish even in infinitely large systems, but instead become sharper. The same is true for any system of particles interacting through potentials that are repulsive at very short ranges and attractive at short-ranges (Lennard–Jones-like systems, or LJ-like for short).

In Section 2 we argue that even though cubic PBC are the most usual choice for numerical simulations due to their simplicity and their low computational cost (see Section 3.1), they're not by any measure the only option available. In particular, we explore cubic, hexagonal-prism and truncated octahedron cells.

In Section 2.2 we show that for large enough LJ-like systems, the most stable configuration is that which minimizes its area. We then analytically search for the minimum surface configuration

as a function of the volume fraction as in [11], but for the three cell geometries described in Section 2.

The predictions of Section 2.2 are shown to be consistent with molecular dynamics simulations of symmetric NM within the framework of the semi-classical model CMD. The model is described in Section 3. Simulations were done at almost zero temperature, at three relevant densities, for two system sizes, and in the three different cell geometries. The results of the simulations themselves are presented and discussed in Section 4.

In addition, and since the motivation for this research is the simulation of NSM, we performed additional simulations with the same model nuclear interaction plus a screened Coulomb potential as a model for NSM. The same model was already used in [9]. Simulations with Coulomb interaction were done at the same temperature and densities, and under all three PBC geometries but for only one size. Results are presented and discussed in Section 5.

We close with some concluding remarks in Section 6.

2. Analytical results in different cell geometries

2.1. Cell geometries

Periodic boundary conditions can be imposed on any polyhedron that fills space by translations. In order to fulfill that requirement, each face must have another face parallel to it and in the exactly opposite side of the cell. This earns this polyhedra the denomination of parallelohedra [43].

In this section we describe the three different unit cells we used in our simulations: cubic, hexagonal prism (HP) and the truncated octahedron (TO) or cubo-octahedron. To quantify the dimensions of each cell we use the distance between the specified pair of opposing faces L_x, where x is C for cubic cell, HP for hexagonal prism cell and TO for the truncated octahedron. As a measure of the 'sphericity' of each cell, we calculate the ratio between s_x the circumsphere radius and the inscribed sphere radius, following [43].

2.1.1. Cube

It's the most commonly used for its simplicity. The cubic cell and its images pack as a simple cubic lattice. It has side length L_c, 6 square faces of area L_c^2 and a volume of $V_C = L_c^3$. The total surface area of the cell is $S_C = 6L_c^2$ and the surface to volume ratio for a unit volume cell is $\frac{S_C}{V_C} = 6$. The ratio between circumsphere and inscribed sphere radii is $s_C = \sqrt{3} \approx 1.73$.

2.1.2. Hexagonal prism

The HP cell has 6 rectangular faces and 2 hexagonal faces (see Fig. 1). It packs in a hexagonal honeycomb in the plane of the hexagonal faces, and stacks evenly along the direction normal to that plane. The HP has a discrete rotational symmetry of order 6 about the axis normal to the hexagonal faces. This symmetry may have an impact which is interesting to explore. We chose its dimensions so that the distance between opposing faces (L_{HP}) is the same for each pair of parallel faces. With these proportions the prism has a height of L_{HP} in the direction normal to the hexagonal faces. The hexagonal faces have area $\frac{\sqrt{3}}{2}L_{HP}^2$ each. The lateral rectangular faces are L_{HP} high and $\frac{\sqrt{3}}{3}L_{HP}$ (their surface area is, then $\frac{\sqrt{3}}{3}L_{HP}^2$).

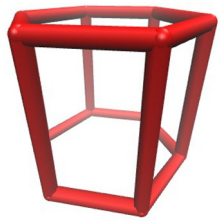

Fig. 1. Hexagonal prism.

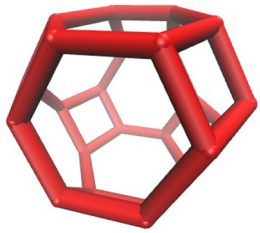

Fig. 2. Truncated octahedron.

The total surface area of the HP is $S_{HP} = 3\sqrt{3}L_{HP}^2$ and its volume $V_{HP} = \frac{\sqrt{3}}{2}L_{HP}^3$. The surface to volume ratio of the HP cell for unit volume is then $\frac{S_{HP}}{V_{HP}} = \frac{6}{L_{HP}}$, which for unit volume is $S_{HP}^1 \approx 5.72$. The ratio between circumsphere and inscribed sphere radii for the HP is $s_{HP} = \sqrt{\frac{7}{3}} \approx 1.53$.

2.1.3. Truncated octahedron

The TO is the Wigner–Seitz cell of the BCC Bravais lattice. As such, it packs as BCC and is inscribed in a cube of side L_{TO}. Also by construction, it has exactly half the volume of this cube: $V_{TO} = \frac{L_{TO}^3}{2}$. The *TO* has 8 hexagonal faces and 6 square faces (see Fig. 2). The distance between each pair of opposing square parallel faces is also L_{TO}, while the distance between opposing hexagonal faces is $\frac{\sqrt{3}}{2}L_{TO}$. The surface area of each hexagonal face is $\frac{3\sqrt{3}L_{TO}^2}{16}$ and for each square face it's $\frac{L_{TO}^2}{8}$. The TO cell's total surface area is $S_{TO} = \frac{3(1+2\sqrt{3})L_{TO}^2}{4}$. Its surface to volume ratio is then $\frac{S_{TO}}{V_{TO}} = \frac{3(1+2\sqrt{3})}{2^{\frac{4}{3}}} \approx 5.31$.

With a value of $s_{TO} = \sqrt{\frac{5}{3}} \approx 1.29$ the TO is the "most spherical" cell of the three.

To summarize, the cubic cell has the largest surface to volume ratio of the three cells, followed by the hexagonal prism and then the truncated octahedron. The cubic cell is also the farthest from spherical of the three. The HP, even if it is closer to spherical than the cube, is less isotropic than the other two. Among these three, the less biasing option seems to be the TO since it's the most spherical, the most isotropic and has the lowest surface to volume ratio. The only advantage of the cubic cell seem to be its computational economy.

2.2. Surface area of usual shapes in other geometries

As we showed in [11], simulations of symmetric NM or LJ-like systems under PBC will produce non-homogeneous structures at $\rho < \rho_0$ and low enough temperature. When using a

Table 1
Surface area for simple shapes under different PBC at volume fraction u and cell of length L_x. L_x^1 is the value of the parameter L_x for which a given cell has unit volume.

	L_x^1	Sphere	Cylinder	Slab
Cube	1	$(6\sqrt{\pi}u)^{\frac{2}{3}} L_C^2$	$\sqrt{4\pi u} L_C^2$	$2L_C^2$
HP	$(\frac{2\sqrt{3}}{3})^{\frac{1}{3}}$	$3(\sqrt{\pi}u)^{\frac{2}{3}} L_{HP}^2$	$\sqrt{\sqrt{12}\pi u} L_{HP}^2$	$\sqrt{3}L_{HP}^2$
TO	$2^{\frac{1}{3}}$	$(3\sqrt{\pi}u)^{\frac{2}{3}} L_{TO}^2$	$\sqrt{\sqrt{3}\pi u} L_{TO}^2$	$\sqrt{2}L_{TO}^2$

cubic cell, shapes are limited to one sphere, one cylindrical rod, one slab or their complementary shapes (cylindrical hole, spherical hole). Except for small transition regions, these shapes exhaust the possible solutions. We also showed that, at a given volume fraction, and for sufficiently large simulations, the equilibrium configuration was that which had the least surface area among these five options. To compute the surface area for each shape we explicitly assumed they were inscribed in a cubic cell under PBC. Because of the PBC, cylinders and slabs formally extend to other cells, thus trading would-be surface for bulk.

In this section we extend those calculations, restricted to the same set of shapes, but now inscribed in each of the three periodic cells described in Section 2.

Jumping ahead, simulations show that rods and slabs favor certain orientations related to the particular symmetries of each cell. For example, rods or tubes pierce the cell orthogonally to some pair of opposing faces, avoiding edges. Moreover, rods (or tubes) at the studied densities are orthogonal to faces of the largest area possible (i.e. the hexagonal faces in both HP and TO, see Section 2). Conversely, slabs are parallel to them. In any case, there is no loss of generality in assuming this scenario. To compute the effective surface area of a rod, for example, we treat it as an open cylinder (without lids) of length L, the distance between faces, and set its radius based on the desired volume fraction. Our calculation has implicitly the additional constraint that the slab is thinner than the side length of the square faces in the TO. Incidentally, that limiting case occurs at volume fraction $u = \frac{1}{2}$, where the slab formally becomes a 'slab-shaped hole'. This constraint is therefore not hampering.

Table 1 shows the analytic expressions for the surface area of the usual simple shapes (sphere, rod, slab) for a given volume fraction u and cell size L. The first column of Table 1 contains the values of L for a cell of unit volume of the corresponding geometry.

We remind the reader that the line of argument is that in absence of Coulomb interaction, the binding energy can be divided into a volume plus a surface (or interface) term:

$$E = a_V V + a_S S \tag{1}$$

In the case of nuclear systems this is nothing more than a truncation of the semi-empirical mass formula. As in [11], we argue that at $T = 0$ the most stable structure is that which minimizes energy, and energy minimization at fixed number density is achieved by surface minimization.

For a more accurate description, the parameters a_V and a_S from Eq. (1) should be functions of the temperature and density. Moreover, since the interaction potentials have finite range, the surface term should be labeled 'interface' term, and at finite temperatures the model should contemplate the presence of a vapor phase in coexistence (see [13]). For large enough systems these corrections fade, as they depend on the surface to volume ratio of the structures. Here we work at $T = 0$, assume saturation density throughout all the occupied volume and ignore interfacial effects. This, of course, is an over-simplified, minimal model. Yet, it captures the essential fea-

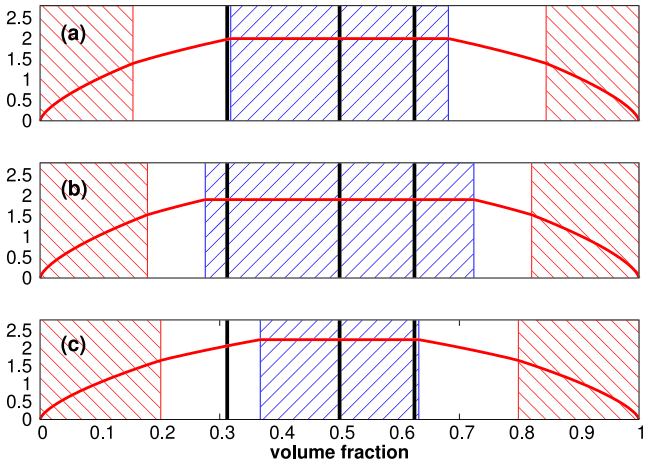

Fig. 3. (Color online.) Least surface area among simple shapes under various PBC for unit volume. Panel (a) for the cubic cell, (b) for the HP cell and panel (c): for the TO cell. Downwards (from left to right) striped (red) areas indicate regions where spheres are the best solution, blank areas indicate regions where cylinders are, and finally, upward striped (blue) areas indicate regions where slabs are the best solution. Solid vertical black lines correspond to the densities used for simulations, assuming local density $\rho_0 = 0.16$ fm (Figs. 4, 5 and 6).

tures needed to understand the underlying mechanism behind the formation of pseudo-pasta and the specific role PBC play.

Having discussed the hypotheses, limitations and scope of the model, we plot in Fig. 3 the least surface area (among those in Table 1) as a function of volume fraction u for the three cell geometries and unit volume cell (see caption for details).

The model yields curves symmetric with respect to $u = 0.5$. In actual simulations of a fixed number of particles, this symmetry is not to be expected for two reasons: on one hand, the approximations implied above are more accurate in the low volume fraction (larger cell) half; that is, for denser systems the surface to volume ratio is smaller and interfacial effects become more important. On the other hand, the finite range of the potentials comes into play again when a structure becomes thick enough to approach its own replicas in a neighboring cell. This amounts to a "lattice energy term" which may further lower the overall energy and prompt the transition between structures at lower values of u than the predicted with this model. The same issue is responsible for the extension of the stability region of pure phases in LJ systems described in [10].

The most evident feature of Fig. 3 is that the regions of stability of each shape are different for each cell geometry. Qualitatively, it's reasonable that the TO should be able to lodge larger spheres or spherical holes than the others: Among the three cells, the TO has the largest distance between replicas. This is reflected in Fig. 3.

It's important to stress that the only physical assumption we made was that only bulk and surface energy contributions are relevant and PBC are imposed. Whenever that is true, (most notably when only LJ-like potentials are involved) these results hold and are fully consistent with those in [13]. More importantly, this is independent of the size of the cell since the surface area of every shape scales with L^2. One should be mindful about this fact when interpreting results from numerical simulations that rely on PBC.

3. Molecular dynamics model

Next we use a classical molecular dynamics model, *CMD* [29], based on the work of V. Pandharipande [30]. It has been very fruitful in studies of heavy ion phenomena: neck fragmentation [31], phase transitions [32], critical phenomena in multifragmentation [33,34], the caloric curve [35,36], and isoscaling [37,38], all without any adjustable parameters. Recently we extended it to be used in the study of NSM [9]. We include here a brief synopsis but readers are directed to these references for further details on the model.

CMD treats nucleons as classical particles interacting through a two-body potential and solves the coupled equations of motion of the many-body system to obtain the trajectories of all particles. Since the $(\mathbf{r}, \mathbf{p})$ information is known for all particles at all times, it's possible to know the structure of the nuclear medium from a particle-wise perspective.

CMD uses the phenomenological potentials developed by Pandharipande [30]:

$$\begin{aligned} V_{np}(r) &= V_r\big[\exp(-\mu_r r)/r - \exp(-\mu_r r_c)/r_c\big] \\ &\quad - V_a\big[\exp(-\mu_a r)/r - \exp(-\mu_a r_c)/r_c\big] \\ V_{nn}(r) &= V_0\big[\exp(-\mu_0 r)/r - \exp(-\mu_0 r_c)/r_c\big], \end{aligned}$$

where V_{np}, the potential between a neutron and a proton, is attractive at large distances and repulsive at small ones. V_{nn} is the interaction between identical nucleons and it's purely repulsive. Notice that no bound state of identical nucleons can exist, and the model produces nuclei consistent with a liquid drop model with a symmetry term [38]. It has many common features with potentials used by other models [6].

The cutoff radius is $r_c = 5.4$ fm after which the potentials are set to zero. Calculations we present in this work were made with the Medium parametrization of the Pandharipande potentials. With this parametrization, symmetric infinite nuclear matter (NM) has an equilibrium density of $\rho_0 = 0.16$ fm^{-3}, a binding energy $E(\rho_0) = 16$ MeV/nucleon and a compressibility of about 250 MeV [30].

As for the Coulomb interaction, we use a screened Coulomb potential of the form

$$V_C^{(Scr)}(r) = \frac{e^2}{r}\exp(-r/\lambda)$$

The correct approximation requires the parameter λ to be the Thomas–Fermi screening length given by

$$\lambda = \left[\frac{\hbar^2(96\pi^2\langle\rho\rangle)^{-1/3}}{me^2}\right]^{1/2}$$

as given in [2], where m is the electron mass, and $\langle\rho\rangle$ is the mean density of the system. The size of the simulation cell should be significantly larger than λ. Since the fulfillment of this requisite leads to prohibitively large systems, it has become a standard to artificially set $\lambda = 10$ fm and use the first image convention to evaluate the forces [4,6]. However, as we discuss in [7], for this model of nuclear interaction a value of $\lambda = 20$ fm is needed to adequately produce the known pasta phenomenology.

The trajectories of individual nucleons are tracked using a Verlet algorithm, and to control the temperature of the system we use an Andersen thermostat [39]. To achieve almost zero temperature, we set the thermostat to successively lower temperatures by small steps, letting the system reach thermal equilibrium at every step until $T = 0.1$ MeV is reached. At that temperature, the

nucleons are almost frozen, but we further cool it to $T = 0.001$ MeV so that thermal fluctuations can be safely neglected.

3.1. Pairwise forces evaluation, cell linked lists and PBC

Before we move on to the results, we deem it worthwhile to discuss the implementation of PBC in MD simulations and the reason behind the almost universal choice of cubic cells.

The most computationally expensive part of an MD code is the evaluation of the pairwise forces acting on all the particles at every time step. The most straightforward and clumsy way to do that is to evaluate the distance r_{ij} between every pair of particles (i, j) and to compute the force when appropriate. This brute–force approach becomes very inefficient for large systems, as the time needed to evaluate the forces scales as N^2. If the forces have a short cutoff radius, as is the case for our NM simulations, there are more clever and efficient ways to perform this evaluation (see [14], for an overview). One of the simplest and most well-known algorithms to do so is the cell-linked lists algorithm. The time needed to evaluate the forces scales as $\mathcal{O}(N^{\frac{3}{2}})$ with this algorithm, but it can only be applied to orthorhombic cells. In a nutshell, the algorithm consists in dividing the simulation cell in regular smaller cells (about the size of r_c) and constructing lists of the particles in each sub-cell. By construction, particles may only interact with other particles which are in the same or in neighboring cells. The use of these lists dramatically reduces the amount of pairs that need to be evaluated if the simulation cell is much larger than the range of the interaction. And, if the effort of constructing the lists does not outweigh this reduction, the overall cost of force evaluation is lowered. In cubic cells this scheme is easily implemented, dividing the cell in smaller cubes, and is very efficient. However it cannot be used in the HP nor in the TO cells since no regular tessellation can be constructed on these geometries.

For our simulations in cubic cells we use cell-linked lists but simulations in the other geometries were only possible thanks to GPU computing. As discussed in [40], for short-ranged interactions, the brute–force algorithm executed massively in parallel on a GPU outperforms the cell-linked lists scheme executed on a single CPU. Our simulations on HP and TO cells were performed using the brute–force algorithm implemented in CUDA [41], the GPU computing platform by NVIDIA, on a GeForce GTX-560 TI GPU with 384 cores [42]. However impressive the performance of the GPU code, the whole cooling procedure for a single density in the TO cell, for example, takes about a week (wall-time) to complete for a system of $A = 4096$. In simulations with Coulomb interaction (Section 5) the scenario is much worse. Even screened, the Coulomb interaction has a much longer range than the nuclear. We chose the number of particles so that the simulation cell is just large enough to use the first image convention for proton–proton interactions. In this case the use of cell-linked lists for the Coulomb interaction does not reduce the run time.

Thus, it is not feasible for us to work with larger systems. On the other hand, we believe that all that is left to be learned from larger simulations is quantitative in nature, and beyond the scope of the present work.

4. Results of simulations without Coulomb interaction

In Section 2.2 we showed, by using simple geometric calculations, that for any system that has only bulk and surface contributions to energy under PBC, the particular geometry of the cell has a great impact on which shape has the least surface area. In those calculations we only considered the three traditional shapes: sphere, rod and slab. While those three shapes almost exhaust the

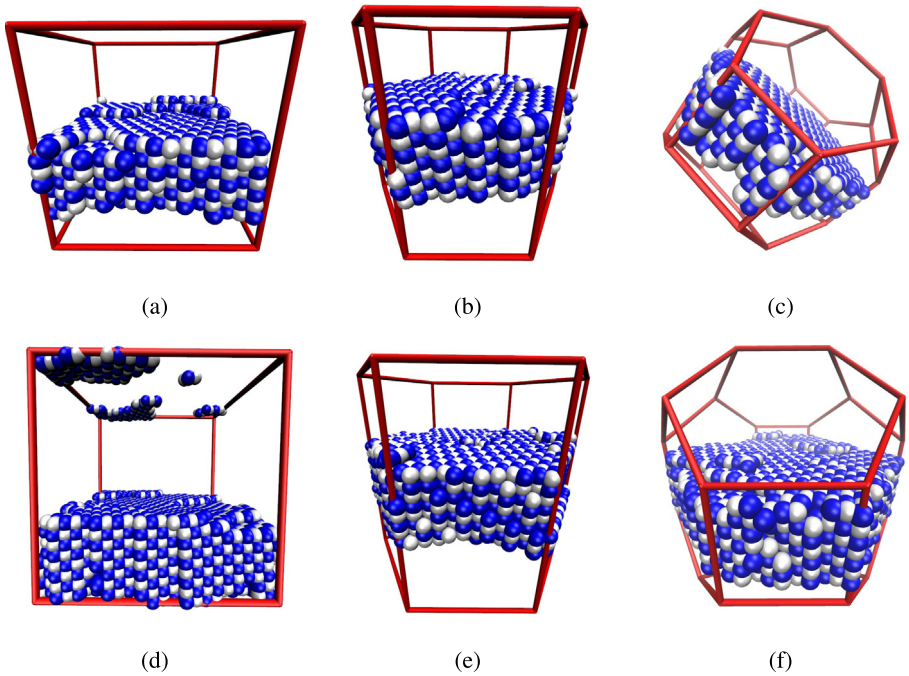

Fig. 4. (Color online.) Configurations at $T = 0.001$ MeV for $A = 1728$ (top row) and $A = 4096$ (bottom row) nucleons at density $\rho = 0.05$ fm^{-3} without Coulomb interaction. Panels (a) and (d) correspond to cubic cells, (b) and (e) to HP cells and panels (c) and (e) to TO cells.

possible results from simulations of large enough Lennard–Jones and NM systems [10,11,13] in cubic cells, it's not clear that these three shapes constitute a representative set of the possible results in other geometries, where different symmetries are imposed.

To test the results from the previous section, and perhaps extend set of possible shapes for PBC other than cubic, we performed molecular dynamics simulations using the three periodic cells described in Section 2. Since volume fraction is intimately related to number density ($u\rho_0 = N/V$), simulations were performed for three densities of interest. Furthermore, to explore how system size effects come into play in each geometry, simulations were made with both $A = 1728$ and $A = 4096$ particles.

In Fig. 4 we show configurations at almost $T = 0$ (see Section 3) for $\rho = 0.05$ fm^{-3} and both sizes. Simulations at this density yield a single slab for every cell.

Our model predicted slabs for the *HP* cell and rods for the other two (see Fig. 3). For the cubic cell this density is very close to the slab region. The interaction between replicas due to the finite range of the interaction potentials is clearly responsible for the discrepancy. The same is true for the *TO*, but it is not so clear. Lets clarify. At this density, the least surface area rod in the *TO* has diameter $d_{rod} \approx 0.48 L_{TO}$ and is lodged in a hexagonal face, which is $w = 0.61 L_{TO}$ wide. For this density and $N = 4096$, the difference between the width of the hexagonal face and the rod's diameter is $w - d_{rod} \approx 7$ fm. That is the distance between replicas of the rod and is almost the cutoff radius of the potential $r_c = 5.4$ fm, so the "true" transition density between rod and slab is closer to the one simulated in Fig. 4 than the one predicted by the model. At the simulated

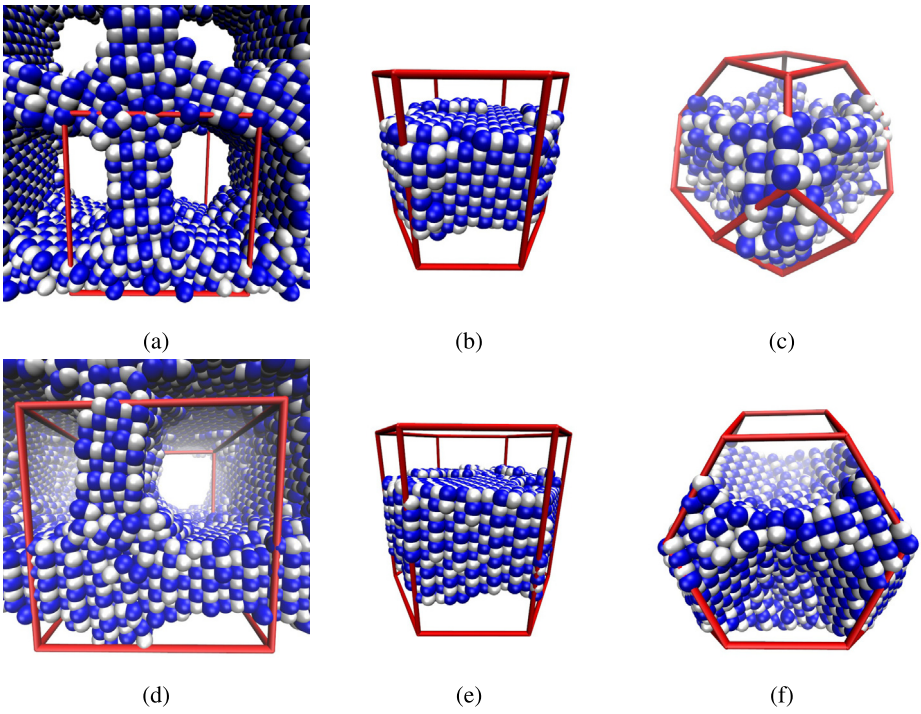

Fig. 5. (Color online.) Configurations at $T = 0.001$ MeV for $A = 1728$ (top row) and $A = 4096$ (bottom row) nucleons at density $\rho = 0.08$ fm^{-3} without Coulomb interaction. Panels (a) and (d) correspond to cubic cells, (b) and (e) to HP cells and panels (c) and (e) to TO cells.

density, the rod should be the ground-state, but thermal fluctuations during the cooling procedure may systematically drive the system to the slab phase.

In Fig. 5 we present results at $\rho = 0.08$ fm^{-3}. At this density, each cell geometry yields a different result: Cylindrical holes for cubic, slabs for HP and spherical holes for TO. There is also no qualitative difference between the shapes found with different system sizes at a given cell geometry. Again, the discrepancy between simulation and model comes from the finite range of the potential, small size and probably hysteresis from the cooling procedure. It's however interesting to observe that these issue further enhance the geometry-dependence of the simulations' results.

Lastly, Fig. 6 shows results at $\rho = 0.10$ fm^{-3}. Again, size has no qualitative effect on the shape that is stable for each geometry but that shape is different in each cell. For cubic and TO the stable shape is a spherical hole and for the HP it's a slab.

The results from this section clearly show that the particular (and *a priori* arbitrary) PBC conditions imposed on an MD simulation of cold nuclear matter (or any system whose energy is mostly a bulk plus a surface term) determines the resulting configurations.

The fact that inhomogeneous solutions exist in simulations with such simple interactions is usually ignored. These simulations yield systematically a single structure per cell, independently of its size and geometry. The length scale of the inhomogeneities is determined by the size of the cell. This means that, no matter how large, simulations of LJ-like systems in the coexistence region will never converge to the thermodynamic limit as predicted by mean field theories such

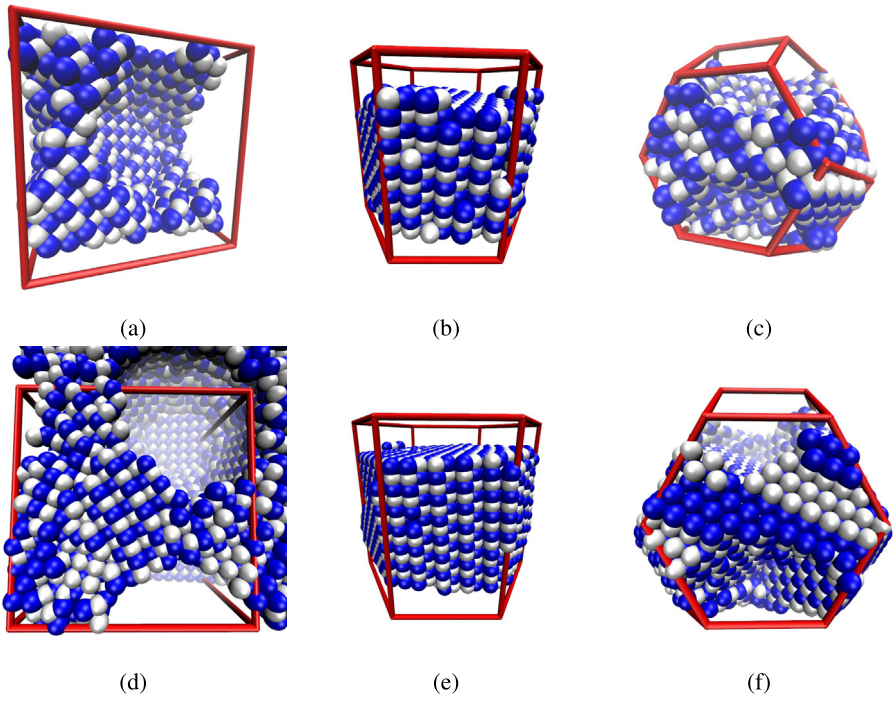

Fig. 6. (Color online.) Configurations at $T = 0.001$ MeV for $A = 1728$ (top row) and $A = 4096$ (bottom row) nucleons at density $\rho = 0.10$ fm^{-3} without Coulomb interaction. Panels (a) and (d) correspond to cubic cells, (b) and (e) to HP cells and panels (c) and (e) to TO cells.

as Van der Waals'. Also, since for very large systems every solution is determined exclusively by surface minimization under the particular PBC, they are solutions to the Plateau's problem [24]. It then becomes obvious that complex non-homogeneous solutions (i.e. not spherical) must inherit a subset of the cell's symmetries, not only its scale, and thus depend on its geometry.

If the system in addition has a competing interaction of a different range, its energy has additional, non negligible terms. Then, surface minimization is not the only mechanism operating to shape the solutions. This competition also give rise to a length scale proper to the interactions. This is why simulations of NSM, which include Coulomb interaction in addition to nuclear, are expected to present several structures per cell. Otherwise there is no guarantee that the solution would not be affected by the boundary conditions, and perhaps some structures implicitly suppressed (see [8,25] for example).

Finite size effects related to the size of the simulation cell are well known but, as far as we know, no one has explored the effects of the cell's geometry and symmetries in the context of NSM simulations before.

5. Results of simulations with Coulomb interaction

In the previous section we analyzed the effect of cell geometry on the possible solutions of NM simulations at sub-saturation densities under PBC. The results from MD simulations were consistent with the simple geometric calculations of Section 2.2. Those calculations assumed that only bulk and surface terms were relevant and thus apply to LJ-like systems. In this section

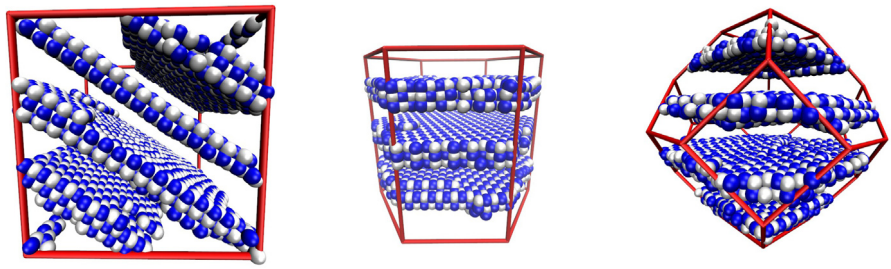

(a) (b) (c)

Fig. 7. (Color online.) Configurations at $T = 0.001$ MeV for $A = 4096$ nucleons at density $\rho = 0.05$ fm^3 with a screened Coulomb interaction in a cubic cell (panel (a)), HP cell (panel (b)) and TO cell (panel (c)).

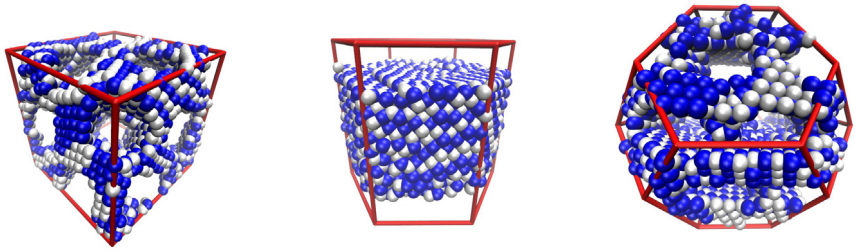

(a) (b) (c)

Fig. 8. (Color online.) Configurations at $T = 0.001$ MeV for $A = 4096$ nucleons at density $\rho = 0.08$ fm^3 with a screened Coulomb interaction. Panels (a) corresponds to a cubic cell, (b) to an HP cells and panel (c) to the TO cell.

perform similar simulations but including a form of Coulomb interaction in the spirit of the Debye approximation (see Section 3), as a model of NSM. As stated before, the screening length must be set to at least $\lambda = 20$ fm (a thorough analysis of this issue is presented in see [7]). Systems of $A = 1728$ particles are too small for this purpose for almost every density studied. And since working with larger systems in the non-cubic cells is beyond our current computational capabilities, we only studied systems of $A = 4096$ particles in the HP and TO cells. In cubic cells simulations were performed also for $A = 9826$ particles. For that size and the densities studied, every cell is large enough.

In Fig. 7 we show results for simulations at $\rho = 0.05$ fm^3 and for the three cell geometries (see figure caption for details) with Coulomb interaction. It can be seen that "lasagna"-like structures are found for every cell. And as expected, more than one per cell.

However, the lasagna found in each cell geometry is different from that of other cells. For example, in the cubic and TO cells (Fig. 7(a) and (b)) there are lasagna of two and three particles wide, but in the HP every slab is three particles wide. Moreover, the distance between slabs is also different in each cell. Under this circumstances it would be unwise to try to extract information about the length scale of density fluctuations without studying larger systems at the same conditions. These differences should become smaller the larger the simulation.

In Fig. 8 we show results for simulations at $\rho = 0.08$ fm^3 for the three cell geometries (see figure caption for details). At this density, both cubic and TO cells consistently yield several cylindrical tubes per cell. In the HP cell, however, the solutions is still a single slab.

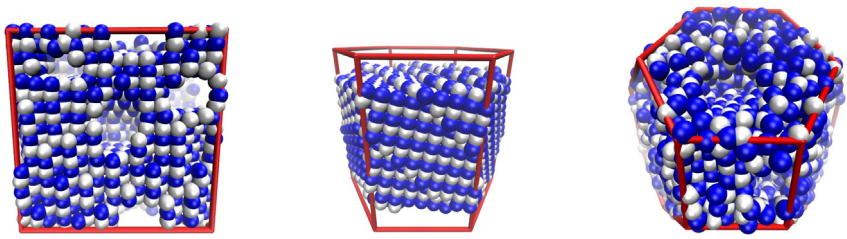

(a) (b) (c)

Fig. 9. (Color online.) Configurations at $T = 0.001$ MeV for $A = 4096$ nucleons at density $\rho = 0.10$ fm^3 with a screened Coulomb interaction. Panels (a) corresponds to a cubic cell, (b) to an HP cells and panel (c) to the TO cell.

At density $\rho = 0.10$ fm^3 (shown in Fig. 9) again the cubic and TO cell yield the same solution (in this case several unconnected holes with no apparent order). But the HP cell still yields a single slab.

It seems that in an HP cell of these proportions, for this system size and at relatively high densities, the mechanism responsible for the formation of non-homogeneous structures without Coulomb interaction (surface minimization exploiting the artificial PBC) is still present. It's present and is strong enough to overwhelm the disrupting effect of Coulomb interaction, which is enough to produce several structures in cells of the same volume but of different geometry. In other words, surface minimization is not frustrated enough in the HP cell. Thus we find that not only the size, but the geometry and symmetries of the cell may affect in unexpected ways the solutions of simulations, even in systems with competing interactions.

We emphasize the fact that finite size effects of PBC manifest in different ways for different cells. Then, having more than one structure per cell is not necessarily enough to guarantee that finite size effects can be ignored. Specially when attempting to extract quantitative information on the scale of density fluctuations from the simulations. However, at lower densities (larger cells) the HP and the TO give approximately the same result as the cubic cell. This means that these effects indeed become smaller the larger the system. As suggested in [25,26], asking for several periods per cell is safer than asking for more than one structure. In any case, these results suggest that for nuclear pasta simulations of this sizes, the actual length scale of density inhomogeneities is set as much by the interaction model as by the size and shape of the simulation cell.

For systems of $A = 9826$ particles in cubic cells, the results are almost the same as for $A = 4096$ particles. In particular, for $\rho = 0.05$ fm^3, the slabs now have a uniform width of three particles (Fig. 10).

We must stress that for larger systems, differences between results in different cells should become smaller, but some may still remain. In the light of our findings without Coulomb interaction, it's likely that the transition densities between different types of pasta may be still depend on the particular cell used for the simulation for larger systems.

6. Concluding remarks

In this work we show that simulations of symmetric NM using a semi-classical model produce non-homogeneous solutions, reminiscent of the "nuclear pasta" expected in NSM, but without a Coulomb interaction. The solutions are shaped as a spherical drop, a cylinder, a slab or their complements (cylindrical or spherical bubble) depending on the number density, but only one per

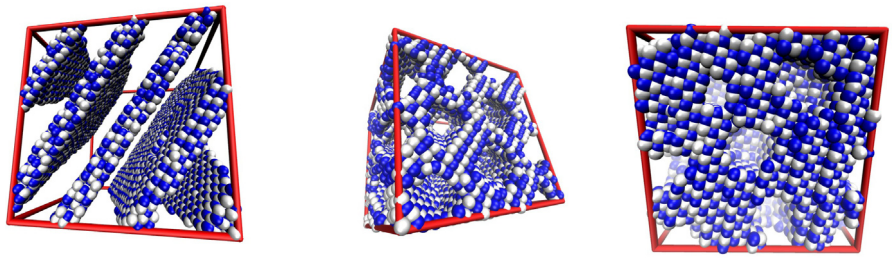

(a) (b) (c)

Fig. 10. (Color online.) Configurations at $T = 0.001$ MeV for $A = 9826$ nucleons with a screened Coulomb interaction at several densities in cubic cells. Panels (a) corresponds $\rho = 0.05$ fm^3, (b) to $\rho = 0.08$ fm^3 and panel (c) to $\rho = 0.10$ fm^3.

simulation cell. By considering only surface and bulk contributions to energy, we show that these non-homogeneous solutions are minimal surface configurations under PBC and, as such, are artificial. We explicitly prove this fact by showing that different primitive cell's geometries produce different solutions at the same physical conditions (i.e. density and temperature). The same is true for any system of particles interacting through Lennard–Jones-like potentials (i.e., short-ranged, attractive and with a hard core). We work at $T = 0$, but results from [13] suggest that at sufficiently low but finite temperatures (namely, sub-critical), this results should approximately describe the behavior of the liquid phase in coexistence.

More importantly, we show that even if this behavior is indeed a finite size effect, it is independent of the actual size of the system (if large enough) and it does not vanish for infinitely large systems.

The core mechanism behind these behavior is that at sub-saturation densities and low enough temperatures, particles tend to coalesce into a single, large, droplet. But as the droplet grows and approaches the size of the cell, it begins to interact with its own replicas in neighboring cells through the artificial PBC. Then, the PBC allows the system to lower its energy by trading would-be surface for bulk, forming what we call pseudo-pasta. The system minimizes its energy by adopting a minimal surface configuration, but the configuration that minimizes the surface at a given volume fraction depends on the cell's geometry and has therefore little physical meaning.

In other words, for LJ-like systems at low temperatures, not only the length scale but also the symmetries of the solution, are set exclusively by the simulation cell. Inhomogeneities are artificial.

On the other hand, if a screened Coulomb interaction is added, a new, physically meaningful length scale appears. This length scale is related to the maximum size an isolated droplet may have before the disruptive effect of the repulsive interaction breaks it down into smaller droplets. The same is true for any system of particles with competing interactions of different ranges. However, even in this case the artificial PBC imposed can bias or constraint the length scale of the inhomogeneities, or even impose symmetries, if the system is not large enough. Our simulations show that this is the case for systems not too large, but often trusted in the context of NSM simulations. For some physical conditions the result depend on the cell used. In particular, for $\rho = 0.08$ fm^{-3}, the cubic and TO cells produce several cylindrical tunnels, yet for the same physical conditions, the HP cell yields a single slab. For $\rho = 0.05$ fm^{-3} (larger cell) the results from every cell are approximately the same. This supports the claim that for larger systems the results would indeed become independent of the simulation cell, as should be expected if data extracted from simulations is to be any good.

In NSM simulations, it is acknowledged that a simulation or model that yields a single structure per cell suffers from unspecified finite size effects. The fact that for the same system size the HP yields a single structure while the cubic and TO produce several, shows that producing multiple structures per cell is, by no means, enough evidence that the solution is free of such effects. Instead, several periods of the non-homogeneous phase should be aimed for.

In general, systems with competing interactions of different ranges have a proper characteristic length scale. The artificial effects discussed in this work will become negligible if the system is large enough, as compared to that scale set by the interactions. Only in this case the inhomogeneities observed will be due to only the interaction potentials and the physical conditions and any kind of finite size effect will be truly negligible.

Acknowledgement

C.O.D. is a member of the "Carrera del Investigador" CONICET supported by CONICET through grant PIP5969.

References

[1] D.G. Ravenhall, C.J. Pethick, J.R. Wilson, Phys. Rev. Lett. 50 (1983) 2066.
[2] R.D. Williams, S.E. Koonin, Nucl. Phys. A 435 (1985) 844.
[3] A.L. Fetter, J.D. Wallecka, Quantum Theory of Many-Particle Systems, McGraw-Hill, 1971.
[4] T. Maruyama, K. Niita, K. Oyamatsu, T. Maruyama, S. Chiba, A. Iwamoto, Phys. Rev. C 57 (1998) 655.
[5] G. Watanabe, K. Sato, K. Yasuoka, T. Ebisuzaki, Phys. Rev. C 66 (2002) 012801.
[6] C.J. Horowitz, M.A. Perez-Garcia, J. Piekarewicz, Phys. Rev. C 69 (2004) 045804.
[7] P.N. Alcain, P.A. Giménez Molinelli, J.I. Nichols, C.O. Dorso, Phys. Rev. C 89 (2014) 055801.
[8] P.N. Alcain, P.A. Giménez Molinelli, C.O. Dorso, arXiv:1406.1550 [nucl-th].
[9] C.O. Dorso, J.A. López, P.A. Giménez Molinelli, Phys. Rev. C 86 (2012) 055805.
[10] K. Binder, B.J. Block, P. Virnau, A. Tröster, Am. J. Phys. 80 (2012) 1009.
[11] P.A. Giménez Molinelli, J.I. Nichols, J.A. López, C.O. Dorso, Nucl. Phys. A 923 (2014) 31–50.
[12] M. Schrader, P. Virnau, K. Binder, Phys. Rev. E 79 (2009) 061104.
[13] L.G. MacDowell, V.K. Shen, J.R. Errington, J. Chem. Phys. 125 (2006) 034705.
[14] D. Frenkel, B. Smit, Understanding Molecular Simulations, 2nd ed., Academic Press, 2002.
[15] G. Watanabe, K. Sato, K. Yasuoka, T. Ebisuzaki, Phys. Rev. C 69 (2004) 055805.
[16] C.J. Horowitz, M.A. Perez-Garcia, D.K. Berry, J. Piekarewicz, Phys. Rev. C 72 (2005) 035801.
[17] W.G. Newton, J.R. Stone, Phys. Rev. C 79 (2009) 055801.
[18] K. Nakasato, K. Oyamatsu, S. Yamada, Phys. Rev. Lett. 103 (2009) 132501.
[19] S. Föster, T. Planterberg, Angew. Chem. Int. Ed. 41 (2002) 688–714.
[20] H. Sonoda, G. Watanabe, K. Sato, K. Yasuoka, T. Ebisuzaki, Phys. Rev. C 77 (2008) 035806.
[21] C. Ortiz, J. Lorenzana, C. Di Castro, Phys. Rev. Lett. 100 (2008) 246402.
[22] J. Archer, C. Ionescu, L. Reatto, J. Phys. Condens. Matter 20 (2008) 415106.
[23] K. Larsson, F. Tiberg, Curr. Opin. Colloid Interface Sci. 9 (2005) 365–369.
[24] W. Gòżdż, R. Holyst, Macromol. Theory Simul. 5 (1996) 321–332.
[25] Minoru Okamoto, Toshiki Maruyama, Kazuhiro Yabana, Toshikata Matsumi, Phys. Lett. B 713 (2012) 284–288.
[26] Minoru Okamoto, Toshiki Maruyama, Kazuhiro Yabana, Toshitaka Tatsumi, Phys. Rev. C 88 (2013) 025801.
[27] H. Pais, J.R. Stone, Phys. Rev. Lett. 109 (2012) 151101.
[28] E.A. Lord, A.L. MacKay, Curr. Sci. 85 (3) (2003) 346–362.
[29] A. Barrañón, C.O. Dorso, J.A. López, J. Morales, Rev. Mex. Fis. 45 (1999) 110.
[30] A. Vicentini, G. Jacucci, V.R. Pandharipande, Phys. Rev. C 31 (1985) 1783;
R.J. Lenk, V.R. Pandharipande, Phys. Rev. C 34 (1986) 177;
R.J. Lenk, T.J. Schlagel, V.R. Pandharipande, Phys. Rev. C 42 (1990) 372.
[31] A. Chernomoretz, L. Gingras, Y. Larochelle, L. Beaulieu, R. Roy, C. St-Pierre, C.O. Dorso, Phys. Rev. C 65 (2002) 054613.
[32] A. Barrañón, C.O. Dorso, J.A. López, Nucl. Phys. A 791 (2007) 222.

[33] A. Barrañón, R. Cárdenas, C.O. Dorso, J.A. López, Heavy Ion Phys. 17 (1) (2003) 41.
[34] C.O. Dorso, J.A. López, Phys. Rev. C 64 (2001) 027602.
[35] A. Chernomoretz, C.O. Dorso, J.A. López, Phys. Rev. C 64 (2001) 044605.
[36] A. Barrañón, J. Escamilla Roa, J.A. López, Phys. Rev. C 69 (2004) 014601.
[37] C.O. Dorso, C.R. Escudero, M. Ison, J.A. López, Phys. Rev. C 73 (2006) 044601.
[38] C.O. Dorso, P.A. Giménez Molinelli, J.A. López, J. Phys. G, Nucl. Part. Phys. 38 (2011) 115101;
C.O. Dorso, P.A. Giménez Molinelli, J.A. López, Rev. Mex. Phys. S57 (1) (2011) 14.
[39] H.C. Andersen, J. Chem. Phys. 72 (1980) 2384.
[40] D.C. Rapaport, Comput. Phys. Commun. 182 (4) (2011) 926–934.
[41] http://www.nvidia.com/object/cuda_home_new.html.
[42] http://www.geforce.com/hardware/desktop-gpus/geforce-gtx-560ti/specifications.
[43] D. Adams, CCP5 Inf. Q. 10 (1983) 30–36.